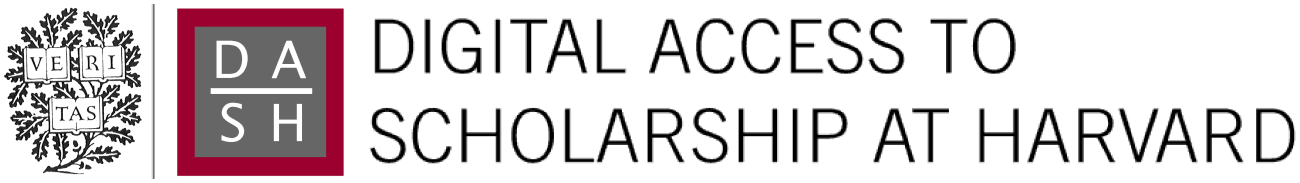

Path Integral Monte Carlo with Importance Sampling for Excitons Interacting with an Arbitrary Phonon Bath

Path integral Monte Carlo with importance sampling for excitons interacting with an arbitrary phonon bath

Sangwoo Shim[1] and Alán Aspuru-Guzik[1]

Department of Chemistry and Chemical Biology, Harvard University, Cambridge, Massachusetts 02138, USA

The reduced density matrix of excitons coupled to a phonon bath at a finite temperature is studied using the path integral Monte Carlo method. Appropriate choices of estimators and importance sampling schemes are crucial to the performance of the Monte Carlo simulation. We show that by choosing the population-normalized estimator for the reduced density matrix, an efficient and physically-meaningful sampling function can be obtained. In addition, the nonadiabatic phonon probability density is obtained as a byproduct during the sampling procedure. For importance sampling, we adopted the Metropolis-adjusted Langevin algorithm. The analytic expression for the gradient of the target probability density function associated with the population-normalized estimator cannot be obtained in closed form without a matrix power series. An approximated gradient that can be efficiently calculated is explored to achieve better computational scaling and efficiency. Application to a simple one-dimensional model system from the previous literature confirms the correctness of the method developed in this manuscript. The displaced harmonic model system within the single exciton manifold shows the numerically exact temperature dependence of the coherence and population of the excitonic system. The sampling scheme can be applied to an arbitrary anharmonic environment, such as multichromophoric systems embedded in the protein complex. The result of this study is expected to stimulate further development of real time propagation methods that satisfy the detailed balance condition for exciton populations.

I. INTRODUCTION

Recent 2D non-linear spectroscopy experiments suggested the existence of long-lived quantum coherence during the electronic energy transfer process within the Fenna-Matthews-Olson complex of green sulfur bacteria, marine algae and plants even under physiological conditions[1–6]. These results attracted a large amount of attention from theoretical physicists and chemists. The energy transfer process usually has been modeled as the dynamics of excitons coupled to a phonon bath in thermal equilibrium within the single exciton manifold. This approximation leads to the famous spin-Boson Hamiltonian. The solution of this type of Hamiltonian has been studied extensively. For example, by assuming a certain relative magnitude between the reorganization energy and coupling terms, one can obtain quantum master equations valid in specific regimes[7–9]. Another approximation, the Haken-Strobl-Reineker model works in both the coherent and incoherent regimes, but incorrectly converges to the high temperature limit in the long time even at the low temperature [10,11]. More recently, numerically exact approaches which interpolate both limits have been investigated and applied to many systems of interest. Two of the most popular methods are the hierarchical equation of motion [12–14] and the quasiadiabatic path integral method[15,16]. These methods are being actively developed, improved, and applied to many systems of interests[17].

Although having been successful in many applications, many of the models described above have assumed the phonon bath to be a set of independent harmonic oscillators and encode all the complexity of the bath environment in the spectral density, which is essentially a frequency dependent distribution of exciton-phonon coupling. However, for studying the anharmonic effects of a very sophisticated bath environment, like the protein complexes of photosynthesis, being able to directly include the atomistic details of the bath structure into the exciton dynamics has a distinct advantage. In other words, approaches that can evaluate the influence functional first suggested by Feynman and Vernon[18] have more straightforward descriptions and are applicable to arbitrary systems. Evaluation of the exact influence functional for arbitrary environment requires the simulation of the full quantum dynamics, which is still not practical with currently available computational resources. There have been several attempts to incorporate atomistic details of the large scale bath by combining the exciton dynamics and molecular dynamics simulations [19–21]. However, these theories are still

in their early stages and the propagation scheme used does not satisfy some fundamental properties, like the detailed balance condition at finite temperature. In pursuit of more accurate theory, it is crucial to know the correct asymptotic behavior in the limit of infinite time. In this context, we decided to explore the numerically exact reduced density matrix in a finite temperature using path integral Monte Carlo[22–25] method. Recently, Moix *et al* applied path integral Monte Carlo for the equilibrium reduced density matrix of the FMO complex within the framework of open quantum systems[26].

II. THEORY

A. Path integral formulation of the reduced thermal density matrix

We want to evaluate the reduced density matrix of an excitonic system coupled to phonons on arbitrary Born-Oppenheimer surfaces at a finite temperature. For photosynthetic energy transfer, we usually restrict the excitons to be within the single exciton manifold because at normal light intensity, in average, one photon is present at a given time in the complexes of interest. However, the formulation itself is not limited to the single exciton manifold. The Hamiltonian operator for such a system can be written as

$$\hat{H} = \underbrace{\sum_m \int d\boldsymbol{R}\ \left[V_m(\boldsymbol{R}) - V_g(\boldsymbol{R})\right] |m\rangle\langle m| \otimes |\boldsymbol{R}\rangle\langle\boldsymbol{R}| + \sum_{m\neq n} \int d\boldsymbol{R}\ J_{mn}(\boldsymbol{R}) |m\rangle\langle n| \otimes |\boldsymbol{R}\rangle\langle\boldsymbol{R}|}_{\hat{H}_{\mathrm{exc}} = \hat{H}_S + \hat{H}_{SB}}$$
$$+ \underbrace{|\mathbf{1}\rangle\langle\mathbf{1}| \otimes \left[\hat{T} + \int d\boldsymbol{R}\ V_g(\boldsymbol{R}) |\boldsymbol{R}\rangle\langle\boldsymbol{R}|\right]}_{\hat{H}_B}. \tag{1}$$

The Hamiltonian was written in terms of the diabatic basis $|m, \boldsymbol{R}\rangle \equiv |m\rangle \otimes |\boldsymbol{R}\rangle$, where m is the index for the exciton state and R is the phonon coordinate. $V_g(\boldsymbol{R})$ is the potential energy surface (PES) of the phonons in the electronic ground state and $V_m(\boldsymbol{R})$ is the PES of the phonons in the mth exciton state. $\hat{T}$ is the kinetic operator of the phonons defined as $\hat{T} = -\frac{\hbar^2}{2}\mathcal{M}^{-1}\nabla^2$, where $\mathcal{M}$ is the mass tensor of the phonons. This expression is generally applicable to any molecular system with multiple potential energy surfaces. The reduced thermal density matrix ρ_S is defined as the partial trace of the full thermal density matrix

with respect to the bath degrees of freedom:

$$\begin{aligned}\rho_S &= \frac{1}{Z(\beta)}\mathrm{Tr_B}\exp\left(-\beta\hat{H}\right)\\ &= \frac{1}{Z(\beta)}\int d\boldsymbol{R}_0\ \langle\boldsymbol{R}_0|\exp\left(-\beta\hat{H}\right)|\boldsymbol{R}_0\rangle,\end{aligned} \tag{2}$$

where $Z(\beta)$ is the partition function of the total system. We proceed by relying on the following identity:

$$\begin{aligned}\langle\boldsymbol{R}_0|\exp(-\beta\hat{H})|\boldsymbol{R}_0\rangle &= \langle\boldsymbol{R}_0|\left\{\exp\left(-\frac{\beta\hat{H}}{M}\right)\right\}^M|\boldsymbol{R}_0\rangle\\ &= \int d\boldsymbol{R}_1\int d\boldsymbol{R}_2\cdots\int d\boldsymbol{R}_{M-1}\\ &\quad\times\langle\boldsymbol{R}_0|\exp\left(-\frac{\beta\hat{H}}{M}\right)|\boldsymbol{R}_{M-1}\rangle\langle\boldsymbol{R}_{M-1}|\exp\left(-\frac{\beta\hat{H}}{M}\right)|\boldsymbol{R}_{M-2}\rangle\cdots\\ &\quad\times\langle\boldsymbol{R}_2|\exp\left(-\frac{\beta\hat{H}}{M}\right)|\boldsymbol{R}_1\rangle\langle\boldsymbol{R}_1|\exp\left(-\frac{\beta\hat{H}}{M}\right)|\boldsymbol{R}_0\rangle.\end{aligned} \tag{3}$$

For any positive integer M, the expression above is exact. When the Trotter decomposition is applied, an imaginary timestep $\tau \equiv \frac{\beta\hbar}{M}$ is usually defined for convenience. Then, the thermal density matrix can be interpreted as an imaginary time evolution. In the limit of an infinitesimal imaginary timestep, the Trotter decomposition converges to the exact result,

$$\begin{aligned}\langle\boldsymbol{R}_1|\exp\left(-\frac{\beta\hat{H}}{M}\right)|\boldsymbol{R}_0\rangle &= \langle\boldsymbol{R}_1|\exp\left(-\tau\hat{H}/\hbar\right)|\boldsymbol{R}_0\rangle\\ &= \langle\boldsymbol{R}_1|e^{-\tau\hat{H}_{\mathrm{exc}}/2\hbar}e^{-\tau\hat{H}_B/\hbar}e^{-\tau\hat{H}_{\mathrm{exc}}/2\hbar}|\boldsymbol{R}_0\rangle + O(\tau^3)\\ &= \int d\boldsymbol{R}_2\int d\boldsymbol{R}_3\ \langle\boldsymbol{R}_1|e^{-\tau\hat{H}_{\mathrm{exc}}/2\hbar}|\boldsymbol{R}_3\rangle\\ &\quad\times\langle\boldsymbol{R}_3|e^{-\tau\hat{H}_B/\hbar}|\boldsymbol{R}_2\rangle\langle\boldsymbol{R}_2|e^{-\tau\hat{H}_{\mathrm{exc}}/2\hbar}|\boldsymbol{R}_0\rangle + O(\tau^3).\end{aligned} \tag{4}$$

Subsequently, we will recast the system part of $\hat{H}_{\mathrm{exc}}$ as a single matrix to simplify the notation,

$$\begin{aligned}\hat{H}_{\mathrm{exc}} &= \sum_{m,n}\int d\boldsymbol{R}\ E_{mn}(\boldsymbol{R})|m\rangle\langle n|\otimes|\boldsymbol{R}\rangle\langle\boldsymbol{R}|,\\ E_{mm}(\boldsymbol{R}) &= \begin{cases} V_m(\boldsymbol{R}) - V_g(\boldsymbol{R}) & for\ \ m = n,\\ J_{mn}(\boldsymbol{R}) & for\ \ m \neq n.\end{cases}\end{aligned} \tag{5}$$

With the single exciton manifold assumption, E_{mm} corresponds to the optical gap of the m-th site. Now, the three terms in the integrand of the Eq. 4 can be written without Dirac notation,

$$\begin{aligned}
\langle \boldsymbol{R}_1|e^{-\tau\hat{H}_{\rm exc}/2\hbar}|\boldsymbol{R}_3\rangle &= \delta(\boldsymbol{R}_1-\boldsymbol{R}_3)e^{-\tau E(\boldsymbol{R}_3)/2\hbar},\\
\langle \boldsymbol{R}_3|e^{-\tau\hat{H}_B/\hbar}|\boldsymbol{R}_2\rangle &= (4\pi\tau|\lambda|)^{-1/2}e^{-\tau V_g(\boldsymbol{R}_3)/2\hbar}e^{-(\boldsymbol{R}_3-\boldsymbol{R}_2)^T\lambda^{-1}(\boldsymbol{R}_3-\boldsymbol{R}_2)/4\tau}e^{-\tau V_g(\boldsymbol{R}_2)/2\hbar}+O(\tau^3),\\
\langle \boldsymbol{R}_2|e^{-\tau\hat{H}_{\rm exc}/2\hbar}|\boldsymbol{R}_0\rangle &= \delta(\boldsymbol{R}_2-\boldsymbol{R}_0)e^{-\tau E(\boldsymbol{R}_0)/2\hbar},
\end{aligned} \tag{6}$$

where $\lambda \equiv \frac{\hbar\mathcal{M}^{-1}}{2}$. By the Eq. 4 and Eq. 6,

$$\begin{aligned}
\langle \boldsymbol{R}_1|\exp\left(-\frac{\beta\hat{H}}{M}\right)|\boldsymbol{R}_0\rangle = (4\pi\tau|\lambda|)^{-1/2}&e^{-\tau V_g(\boldsymbol{R}_1)/2\hbar}e^{-(\boldsymbol{R}_1-\boldsymbol{R}_0)^T\lambda^{-1}(\boldsymbol{R}_1-\boldsymbol{R}_0)/4\tau}e^{-\tau V_g(\boldsymbol{R}_0)/2\hbar}\\
&\times e^{-\tau E(\boldsymbol{R}_1)/2\hbar}e^{-\tau E(\boldsymbol{R}_0)/2\hbar}+O(\tau^3).
\end{aligned} \tag{7}$$

Note that Eq. 7 is a matrix with the same dimension as the reduced density matrix of the system. Substituting Eq. 7 to Eq. 2, we obtain

$$\begin{aligned}
\rho_S = &\frac{1}{Z(\beta)}\int d\boldsymbol{R}_0\int d\boldsymbol{R}_1\cdots\int d\boldsymbol{R}_{M-1}\\
&\times e^{-\tau E(\boldsymbol{R}_0)/2\hbar}e^{-\tau E(\boldsymbol{R}_{M-1})/\hbar}\cdots e^{-\tau E(\boldsymbol{R}_1)/\hbar}e^{-\tau E(\boldsymbol{R}_0)/2\hbar}\\
&\times e^{-\tau V_g(\boldsymbol{R}_0)/\hbar}e^{-\tau V_g(\boldsymbol{R}_1)/\hbar}\cdots e^{-\tau V_g(\boldsymbol{R}_{M-1})/\hbar}\\
&\times e^{-(\boldsymbol{R}_0-\boldsymbol{R}_{M-1})^T\lambda^{-1}(\boldsymbol{R}_0-\boldsymbol{R}_{M-1})/4\tau}e^{-(\boldsymbol{R}_{M-1}-\boldsymbol{R}_{M-2})^T\lambda^{-1}(\boldsymbol{R}_{M-1}-\boldsymbol{R}_{M-2})/4\tau}\\
&\times\cdots\times e^{-(\boldsymbol{R}_1-\boldsymbol{R}_0)^T\lambda^{-1}(\boldsymbol{R}_1-\boldsymbol{R}_0)/4\tau}\\
=&\int d\boldsymbol{R}_0\int d\boldsymbol{R}_1\cdots\int d\boldsymbol{R}_{M-1}\\
&\times\underbrace{\frac{K}{Z(\beta)}e^{-\tau E(\boldsymbol{R}_0)/2\hbar}e^{-\tau E(\boldsymbol{R}_{M-1})/\hbar}\cdots e^{-\tau E(\boldsymbol{R}_1)/\hbar}e^{-\tau E(\boldsymbol{R}_0)/2\hbar}}_{\rho_{\rm PIMC}(\boldsymbol{R}_0,\cdots,\boldsymbol{R}_{M-1})}\\
&\times\underbrace{\frac{1}{K}e^{-\beta V_{\rm PIMC}(\boldsymbol{R}_0,\boldsymbol{R}_1,\cdots,\boldsymbol{R}_{M-1})}}_{f_g(\boldsymbol{R}_0,\cdots,\boldsymbol{R}_{M-1})},
\end{aligned} \tag{8}$$

where,

$$\begin{aligned}
V_{\rm PIMC}(\boldsymbol{R}_0,\boldsymbol{R}_1,\cdots,\boldsymbol{R}_{M-1}) = &\frac{1}{M}\sum_{i=0}^{M-1}V_g(\boldsymbol{R}_i)\\
&+\sum_{i=0}^{M-1}\frac{M}{2\beta^2\hbar^2}\{\boldsymbol{R}_i-\boldsymbol{R}_{{\rm mod}(i+1,M)}\}^T\mathcal{M}\{\boldsymbol{R}_i-\boldsymbol{R}_{{\rm mod}(i+1,M)}\}.
\end{aligned} \tag{9}$$

The expressions above show that the reduced thermal density matrix ρ_S can be evaluated as an expectation value of $\rho_{\mathrm{PIMC}}(\boldsymbol{R}_0, \cdots, \boldsymbol{R}_{M-1})$ where the joint probability density function of the M N-dimensional random variables $(\boldsymbol{R}_0, \cdots, \boldsymbol{R}_{M-1})$ is f_g. This type of multidimensional integral can be efficiently evaluated using Monte Carlo integration. Because $f_g(\boldsymbol{R}_0, \cdots, \boldsymbol{R}_{M-1})$ is invariant to cyclic permutation of the phonon coordinate, usually the averaged estimator ρ_{PIMC} over the cyclic permutation is used in the actual Monte Carlo evaluation:

$$\rho_{\overline{\mathrm{PIMC}}} = \frac{1}{M} \sum_{i=0}^{M-1} \rho_{\mathrm{PIMC}}(\boldsymbol{R}_i, \boldsymbol{R}_{\mathrm{mod}(i+1,M)}, \cdots, \boldsymbol{R}_{\mathrm{mod}(i+M-1,M)}). \tag{10}$$

B. Population-normalized estimator and importance sampling

In the previous approach described in Eq. 8, the phonon coordinates are sampled according the electronic ground state PES. The estimator should converge to the target quantity in the long time limit, taking into account the discretization error. As long as $f_g(\boldsymbol{R}_0, \cdots, \boldsymbol{R}_{M-1})$ is positive definite everywhere in the phonon space, the sampling efficiency depends on the selection of the probability density. Obviously, the actual distribution of the phonon coordinate depends heavily on the excited state PES. Therefore, the Monte Carlo points coordinates sampled according to the reduced dynamics of the bath by taking the partial trace with respect to the *exciton degrees of freedom*, as explored in multiple surface path integral Monte Carlo approaches, are expected to give the better estimates. This choice of the probability density reweights the estimator in the following way:

$$\begin{aligned} f_I(\boldsymbol{R}_0, \cdots, \boldsymbol{R}_{M-1}) &= \mathrm{Tr}_{\mathrm{S}} \left[\rho_{\overline{\mathrm{PIMC}}}(\boldsymbol{R}_0, \cdots, \boldsymbol{R}_{M-1})\right] f_g(\boldsymbol{R}_0, \cdots, \boldsymbol{R}_{M-1}), \\ \rho_I(\boldsymbol{R}_0, \cdots, \boldsymbol{R}_{M-1}) &= \frac{\rho_{\overline{\mathrm{PIMC}}}(\boldsymbol{R}_0, \cdots, \boldsymbol{R}_{M-1})}{\mathrm{Tr}_{\mathrm{S}} \left[\rho_{\overline{\mathrm{PIMC}}}(\boldsymbol{R}_0, \cdots, \boldsymbol{R}_{M-1})\right]}. \end{aligned} \tag{11}$$

In the expression above, we call $\rho_I(\boldsymbol{R}_0, \cdots, \boldsymbol{R}_{M-1})$ the population normalized estimator for the reduced density matrix because the sum of its populations is always constrained to be 1. The effective energy gap term of $-\frac{1}{\beta} \log \mathrm{Tr} \rho_{\overline{\mathrm{PIMC}}}(\boldsymbol{R}_0, \cdots, \boldsymbol{R}_{M-1})$ was added to the Eq. 9 to enable the phonons follow the excited state dynamics depending on the exciton state ρ_S. For the estimator of the reduced density matrix in Eq. 8, the normalization must obtained by the estimates of its diagonal elements, leading to more uncertainties in the coherence. However, the population-normalized estimator preserves the correct normalization by construction, and does not suffer from any additional uncertainty.

Local gradient information can improve the efficiency and scaling of the sampling procedure by means of a gradient-based approach such as the Metropolis-adjusted Langevin algorithm (MALA).[27,28] However, the exact closed form of the gradient of the effective energy gap term, $\log \mathrm{Tr_S} \rho_{\overline{\mathrm{PIMC}}}(\boldsymbol{R}_0, \cdots, \boldsymbol{R}_{M-1})$ can only be expressed as a function of a power series of matrices. Nevertheless, with the following approximation:

$$\sum_{k=0}^{n} A^k B A^{n-k} \approx \sum_{k=0}^{n} \frac{1}{2^n} \binom{n}{k} A^k B A^{n-k}, \tag{12}$$

an accurate approximated of the gradient can be obtained and employed in the sampling procedure,

$$\begin{aligned}
\frac{\partial}{\partial R_{ij}} \log \mathrm{Tr_S}\left[\rho_{\overline{\mathrm{PIMC}}}(\boldsymbol{R}_0, \cdots, \boldsymbol{R}_{M-1})\right] &= \frac{\mathrm{Tr_S}\left[\frac{\partial}{\partial R_{ij}} \rho_{\overline{\mathrm{PIMC}}}(\boldsymbol{R}_0, \cdots, \boldsymbol{R}_{M-1})\right]}{\mathrm{Tr_S}\left[\rho_{\overline{\mathrm{PIMC}}}(\boldsymbol{R}_0, \cdots, \boldsymbol{R}_{M-1})\right]} \\
&\approx \frac{\mathrm{Tr_S}\left[-\frac{\tau}{2\hbar} \frac{\partial E(\boldsymbol{R}_i)}{\partial R_{ij}} \rho_{\overline{\mathrm{PIMC}}}(\boldsymbol{R}_0, \cdots, \boldsymbol{R}_{M-1})\right]}{\mathrm{Tr_S}\left[\rho_{\overline{\mathrm{PIMC}}}(\boldsymbol{R}_0, \cdots, \boldsymbol{R}_{M-1})\right]}, \\
\nabla_i \log f_g(\boldsymbol{R}_0, \cdots, \boldsymbol{R}_{M-1}) &= -\frac{\beta}{M} \nabla_i V_g(\boldsymbol{R}_i) \\
&\quad + \frac{M}{2\beta\hbar^2} \mathcal{M}(\boldsymbol{R}_{\mathrm{mod}(i+1,M)} + \boldsymbol{R}_{\mathrm{mod}(i-1,M)} - 2\boldsymbol{R}_i), \\
\mu_i(\boldsymbol{R}_0, \cdots, \boldsymbol{R}_{M-1}) &= \frac{\mathrm{Tr_S}\left[-\frac{\tau}{2\hbar} \frac{\partial E(\boldsymbol{R}_i)}{\partial R_{ij}} \rho_{\overline{\mathrm{PIMC}}}(\boldsymbol{R}_0, \cdots, \boldsymbol{R}_{M-1})\right]}{\mathrm{Tr_S}\left[\rho_{\overline{\mathrm{PIMC}}}(\boldsymbol{R}_0, \cdots, \boldsymbol{R}_{M-1})\right]} \\
&\quad + \nabla_i \log f_g(\boldsymbol{R}_0, \cdots, \boldsymbol{R}_{M-1}) \\
&\approx \nabla_i \log f_I(\boldsymbol{R}_0, \cdots, \boldsymbol{R}_{M-1}).
\end{aligned} \tag{13}$$

Here, ∇_i is the gradient operator with respect to $\boldsymbol{R}_i$.

Note that if we choose an appropriate Metropolis criterion, no bias in the distribution is introduced even with the approximate gradient[29]. Firstly, a trial move $\boldsymbol{R}_i'$ obtained by

$$\boldsymbol{R}_i' = \boldsymbol{R}_i + \mu_i(\boldsymbol{R}_0, \cdots, \boldsymbol{R}_{M-1})\Delta t + \xi_i \sqrt{\Delta t}, \tag{14}$$

where Δt is the timestep for the Monte Carlo step and ξ_i is a N-dimensional vector of independent standard Gaussian random variables. Then, R_i' is probabilistically accepted according to the acceptance ratio,

$$\frac{f_I(\boldsymbol{R}_0', \cdots, \boldsymbol{R}_{M-1}')}{f_I(\boldsymbol{R}_0, \cdots, \boldsymbol{R}_{M-1})} \times \frac{\prod_{i=0}^{M-1} \exp\left[-\frac{|\boldsymbol{R}_i' - \{\boldsymbol{R}_i + \mu_i(\boldsymbol{R}_0, \cdots, \boldsymbol{R}_{M-1})\}|^2}{2\Delta t}\right]}{\prod_{i=0}^{M-1} \exp\left[-\frac{|\boldsymbol{R}_i - \{\boldsymbol{R}_i' + \mu_i(\boldsymbol{R}_0', \cdots, \boldsymbol{R}_{M-1}')\}|^2}{2\Delta t}\right]}. \tag{15}$$

The Monte Carlo timestep Δt is only a tunable parameter for the Monte Carlo sampling procedure and not related to the physics of the simulated system.

Parameters	Value
k_{11}	4×10^{-5}
k_{22}	3.2×10^{-5}
x_{11}	7
x_{22}	10.5
ε_{11}	0
ε_{22}	2.2782×10^{-5}
c	5×10^{-5}
α	0.4
x_{12}	8.75
m	3.6743×10^{3}

TABLE I. Summary of the parameters for the model system by Alexander *et al*[30]. All values are given in atomic units.

III. APPLICATION

A. Alexander's 1D test model

Our formulation is equivalent to the multiple electronic state extension of matrix multiplication path integral (MMPI) method of Alexander[22,30] when the population normalized estimator is chosen and only the vibrational degrees of freedom are considered. Therefore, the 1D model employed in Ref. 30 was calculated to test the validity of our method. The elements of the electronic Hamiltonian in this model are given by,

$$\begin{aligned} V_{11}(x) &= \frac{1}{2}k_{11}(x - x_{11})^2 + \varepsilon_{11}, \\ V_{22}(x) &= \frac{1}{2}k_{22}(x - x_{22})^2 + \varepsilon_{22}, \\ V_{12}(x) &= c \exp\left[-\alpha(x - x_{12})^2\right], \end{aligned} \tag{16}$$

The total nuclear probability density evaluated as histograms from the Metropolis random walk and MALA simulations are compared to the grid-based result from Alexander *et al.*[30] in Fig. 1. The distributions converged to the exact probability density after 2×10^7 steps with 8 beads at both temperatures of 8K and 30K.

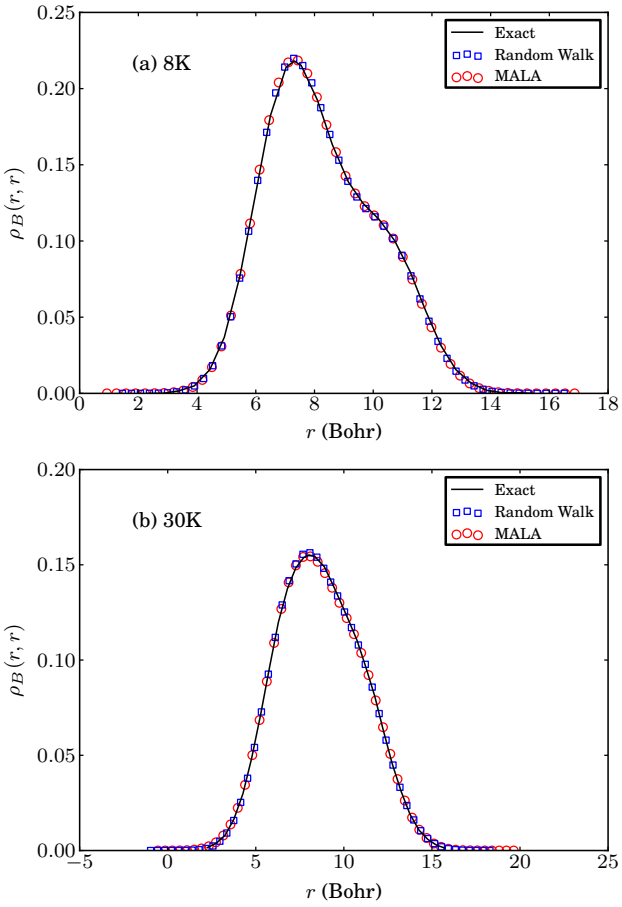

FIG. 1. The estimated nuclear probability densities of Alexander's model[30] at (a) 8K and (b) 30K. For path integral Monte Carlo simulations, densities were obtained by histograms with 50 bins. The discretization number of 8 was enough to converge to the exact probability densitiies.

B. Model of a chromophore heterodimer with displaced harmonic oscillators

To test the proposed method, a system of two chromophores in a photosynthetic complex was modeled using displaced harmonic oscillator model. In this model, the ground and excited electronic states of the monomer are modeled as harmonic oscillators with different displacement, but the same harmonic constant[8]. The thermal reduced density matrix was calculated within the single exciton manifold. The Hamiltonian for this model is then given

Parameter	Value
k_1	2.227817×10^{-3}
k_2	2.227817×10^{-3}
d_1	3.00000
d_2	2.00000
ε_1	8.064745×10^{-2}
ε_2	7.976238×10^{-2}
J	-4.738588×10^{-4}
m_1	3.418218×10^{6}
m_2	3.418218×10^{6}

TABLE II. Summary of the parameters for the displaced harmonic oscillator model used in Sec. III B. All values are given in atomic units.

as follows:

$$
\begin{aligned}
V_g(x_1, x_2) &= \frac{1}{2}(k_1 x_1^2 + k_2 x_2^2), \\
V_e(x_1, x_2) &= \begin{pmatrix} \frac{1}{2}k_1\{(x_1 - d_1)^2 - x_1^2\} + \varepsilon_1 & J \\ J & \frac{1}{2}k_2\{(x_2 - d_2)^2 - x_2^2 + \varepsilon_2\} \end{pmatrix}, \\
\mathcal{M} &= \begin{pmatrix} m_1 & 0 \\ 0 & m_2 \end{pmatrix}.
\end{aligned} \tag{17}
$$

Some of the parameters were set according to our molecular dynamics/quantum chemistry calculation of the FMO complex[19]. The parameter values are listed in table II.

The model system was simulated at seven different temperatures ranging from 30K to 300K with a number of beads (discretization number) of 4, 8, 16, 32 and 64. The number of timesteps propagated in each simulation was 4×10^7. The value of each timestep was tuned so that the acceptance ratio of the MALA run is close to 0.574, and 0.234 for the Metropolis random walk as maintaining these acceptance ratio is known to provide most efficient sampling[28]. We used non-overlapping batch means[31] with a batch size of 10^6 to estimate the standard error of the correlated samples. The batch size was adjusted so that the null hypothesis of uncorrelated batches was not rejected by using Ljung-Box test[32] at a significance level of 5%.

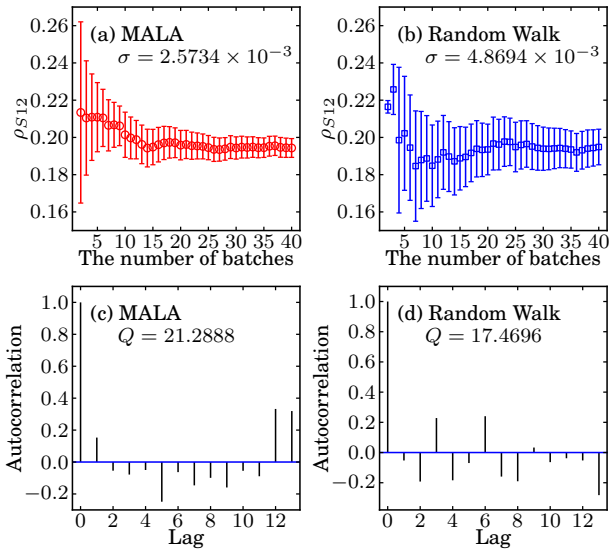

FIG. 2. Estimates of (1,2) matrix elements of the thermal reduced density matrix evaluated using MALA and Metropolis random walk at 77K with 64 beads. MALA estimate has a smaller confidence interval thus a more accurate estimate than that of the Metropolis random walk. The error bar indicates the 95% confidence interval evaluated with the batch means. The 0.95 quantile of the χ^2 distribution with 13 degrees of freedom is 22.362 and both Ljung-Box statistics (Q) are smaller. Thus, the uncorrelation hypothesis is not rejected in both cases at the 5% significance level.

As shown in Fig. 2, the standard error of the simulation decreases modestly as the number of Monte Carlo steps increases. Fig. 3 shows the temperature dependence of the estimates of reduced density matrix elements as a function of various discretization numbers using MALA. Although the Metropolis random walk simulation gives a smaller confidence interval for the 4 bead case, MALA provides better estimates as the dimension of the sample space increases. The Metropolis random walk result is given in Fig. 4. While the population of the low energy site decreases as the temperature increases, the quantum coherence does not monotonically decrease. We believe that this pheonomenon is an artifact of an insufficient discretization number at low temperatures. As can be seen in Fig. 3, 64 or more beads are needed for the coherence to converge at 77K, while 16 beads are enough at 300K with acceptable accuracy. This is a well known limition of imaginary time path integral Monte Carlo simulations. Figure 5 shows the probability density function of the phonon coordinate at 77K and 300K. The population difference in the reduced density matrix is reflected to

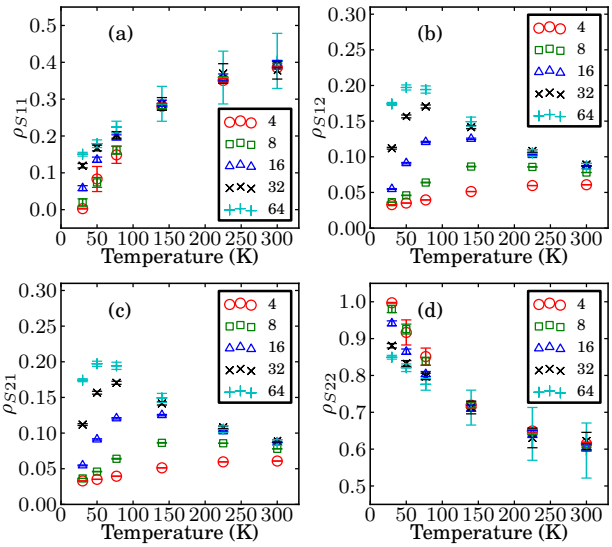

FIG. 3. Estimates of matrix elements of the thermal reduced density matrix evaluated at 30K, 50K, 77K, 140K, 225K and 300K with different discretization numbers of 4, 8 and 16 using MALA. (a) is the (1,1) element, (b), (c) and (d) are (1,2), (2,1) and (2,2) elements, respectively. The error bar indicates the 95% confidence interval evaluated with the batch means.

the difference in the probability mass of the two diabatic potential energy minimum at $(3, 0)$ and $(0, 2)$.

IV. CONCLUSION

We explore a method for obtaining the thermal reduced density matrix of an exciton system coupled to an arbitrary phonon bath for path integral Monte Carlo simulation. Note that our scheme is closely related to the path integral Monte Carlo simulation for nonadiabatic systems for vibrational coherence[30,33,34]. Although the phonon state can be obtained as a byproduct, we mainly focused on the evaluation of the reduced density matrix of the excitonic system to explore the asymptotic behavior of the populations and coherences in this paper. In addition, we implemented an importance sampling scheme for better spatial scaling and sampling efficiency. Although the path integral Monte Carlo cannot evaluate the real time evolution of density matrices, the method gives the exact asymptotic values with all quantum effects from both the system and bath environments if a sufficient number of beads are used. We believe that in some of the cases where the bath has a nontrivial coupling

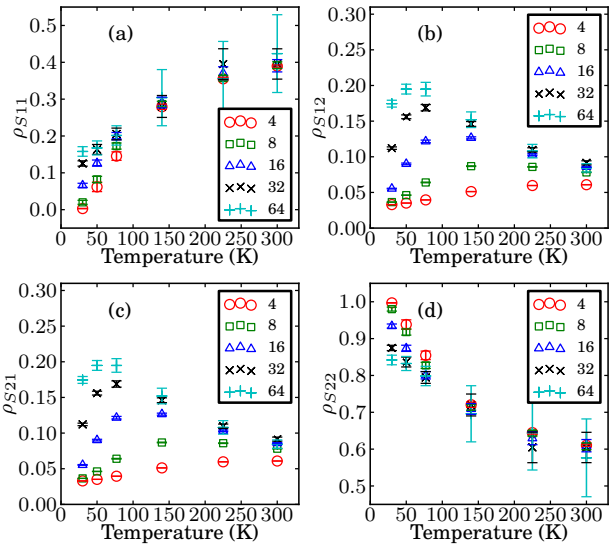

FIG. 4. Estimates of matrix elements of the thermal reduced density matrix evaluated at 30K, 50K, 77K, 140K, 225K and 300K with different discretization numbers of 4, 8 and 16 using random walk Metropolis. (a) is the (1,1) element, (b), (c) and (d) are (1,2), (2,1) and (2,2) elements, respectively. The error bar indicates the 95% confidence interval evaluated with the batch means.

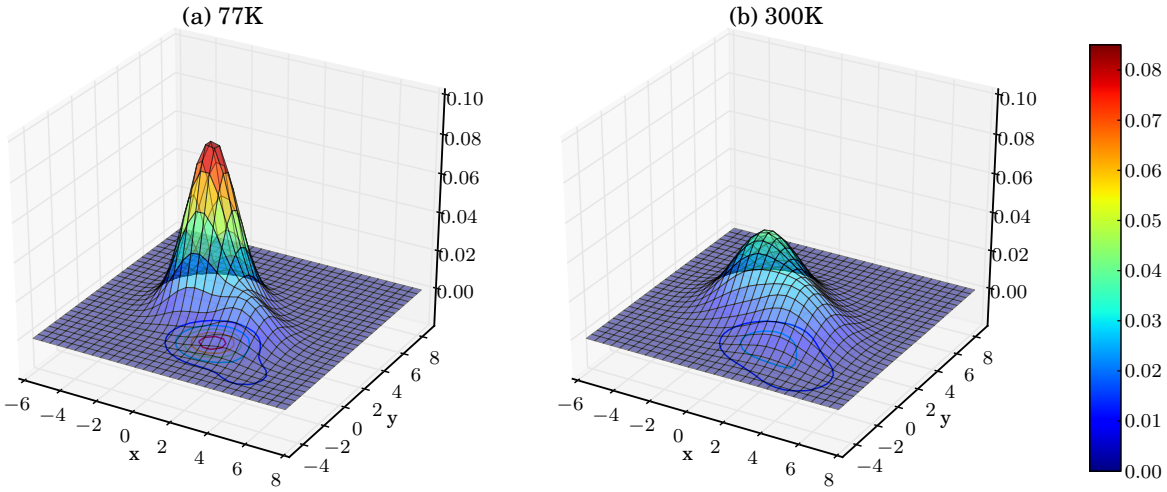

FIG. 5. The phonon probability density function evaluated at (a) 77K and (b) 300K with 16 beads using MALA. At the lower temperature, the contribution of the exciton with lower energy at $(0, 2)$ becomes larger. Therefore, the population differenece becomes more distinct, as can be seen in the temperature dependence of the exciton population in Fig. 3.

to the system, or the non-Markovianity of the bath manifests very strongly, treating the environment around the system of interest as a set of harmonic oscillators is not sufficient. If this is the case, the system should be studied in its entirety. We are trying to develop a real time propagation scheme to treat the system exactly, and the bath semiclassically. The method studied in this paper offers a foundation for it by providing the correct asymptotic behaviors.

ACKNOWLEDGMENTS

S.S. thanks the Samsung Scholarship for financial support. This work was supported by the Defense Advanced Research Project Agency Award No. N66001-10-4060 and by the Center of Excitonics, and Energy Frontier Research Center funded by the U.S. Department of Energy, Office of Science, and Office of Basic Energy Sciences under Award No. desc0001088. A.A.-G. also acknowledges generous support from the Alfred P. Sloan and the Camille and Henry Dreyfus foundations.

REFERENCES

[1]G. S. Engel, T. R. Calhoun, E. L. Read, T.-K. Ahn, T. Mancal, Y.-C. Cheng, R. E. Blankenship, and G. R. Fleming, *Nature.* **446**, 782 (2007).

[2]G. Panitchayangkoon, D. Hayes, K. A. Fransted, J. R. Caram, E. Harel, J. Wen, R. E. Blankenship, and G. S. Engel, *Proc. Natl Acad. Sci. USA.* **107**, 12766 (2010).

[3]G. S. Schlau-Cohen, A. Ishizaki, T. R. Calhoun, N. S. Ginsberg, M. Ballottari, R. Bassi, and G. R. Fleming, *Nat. Chem.* **advance online publication.** (2012).

[4]C. Y. Wong, R. M. Alvey, D. B. Turner, K. E. Wilk, D. A. Bryant, P. M. G. Curmi, R. J. Silbey, and G. D. Scholes, *Nat. Chem.* **advance online publication.** (2012).

[5]E. Collini, C. Y. Wong, K. E. Wilk, P. M. G. Curmi, P. Brumer, and G. D. Scholes, *Nature.* **463**, 644 (2010).

[6]A. Kolli, E. J. O'Reilly, G. D. Scholes, and A. Olaya-Castro, The fundamental role of localised vibrations in excitation dynamics in photosynthetic light-harvesting systems, arXiv:1203.5056v1, 2012.

[7]T. Föster, *Ann. Phys.* **437**, 55 (1948).

[8]V. May and O. Kühn, *Charge and Energy Transfer Dynamics in Molecular Systems*, Wiley-VCH Verlag, Weinheim, 2004.

[9]A. G. Redfield, *IBM J. Res. Dev.* **1**, 19 (1957).

[10]H. Haken and P. Reineker, *Z. Phys.* **249**, 253 (1972).

[11]H. Haken and G. Strobl, *Z. Phys.* **262**, 135 (1973).

[12]A. Ishizaki and Y. Tanimura, *J. Phys. Soc. Jpn* **74**, 3131 (2005).

[13]A. Ishizaki and G. R. Fleming, *J. Chem. Phys.* **130**, 234111 (2009).

[14]A. Ishizaki and G. R. Fleming, *Proc. Natl Acad. Sci. USA.* **106**, 17255 (2009).

[15]M. Topaler and N. Makri, *J. Chem. Phys.* **97**, 9001 (1992).

[16]N. Makri, *Chem. Phys. Lett.* **193**, 435 (1992).

[17]J. Zhu, S. Kais, P. Rebentrost, and A. Aspuru-Guzik, *J. Phys. Chem. B.* **115**, 1531 (2011).

[18]R. Feynman and F. Vernon, *Ann. Phys.* **24**, 118 (1963).

[19]S. Shim, P. Rebentrost, S. Valleau, and A. Aspuru-Guzik, *Biophys. J.* **102**, 649 (2012).

[20]C. Olbrich and U. Kleinekathofer, *J. Phys. Chem. B.* **114**, 12427 (2010).

[21]C. Olbrich, J. Strümpfer, K. Schulten, and U. Kleinekathöfer, *J. Phys. Chem. B* **115**, 758 (2011).

[22]D. Thirumalai, E. J. Bruskin, and B. J. Berne, *J. Chem. Phys.* **79**, 5063 (1983).

[23]K. Allinger, B. Carmeli, and D. Chandler, *J. Chem. Phys.* **84**, 1724 (1986).

[24]E. C. Behrman, G. a. Jongeward, and P. G. Wolynes, *J. Chem. Phys.* **83**, 668 (1985).

[25]J. Cao and B. J. Berne, *J. Chem. Phys.* **99**, 2902 (1993).

[26]J. M. Moix, Y. Zhao, and J. Cao, *Phys. Rev. B* **85**, 115412 (2012).

[27]C. P. Robert and G. Casella, *Monte Carlo statistical methods.*, Springer Verlag, New York, 2004.

[28]N. S. Pillai, A. M. Stuart, and A. H. Thiery, Optimal Scaling and Diffusion Limits for the Langevin Algorithm in High Dimensions, arXiv:1103.0542v2, 2011.

[29]A. Aspuru-Guzik and W. A. Lester Jr., Quantum Monte Carlo methods for the solution of the Schrdinger equation for molecular systems, in *Special Volume, Computational Chemistry*, edited by C. L. Bris, volume 10 of *Handbook of Numerical Analysis*, pp. 485 – 535, Elsevier, 2003.

[30]M. H. Alexander, *Chem. Phys. Lett.* **347**, 436 (2001).

[31]J. M. Flegal and G. L. Jones, *Ann. Stat.* **38**, 1034 (2010).

[32]G. M. Ljung and G. E. P. Box, *Biometrika.* **65**, 297 (1978).

[33]C. D. Schwieters and G. a. Voth, *J. Chem. Phys.* **111**, 2869 (1999).

[34]J. R. Schmidt and J. C. Tully, *J. Chem. Phys.* **127**, 094103 (2007).